Open Archive TOULOUSE Archive Ouverte (OATAO)

OATAO is an open access repository that collects the work of Toulouse researchers and makes it freely available over the web where possible.

This is an author-deposited version published in : http://oatao.univ-toulouse.fr/
Eprints ID : 10368

Any correspondance concerning this service should be sent to the repository administrator: staff-oatao@listes-diff.inp-toulouse.fr

Numerical simulation of a 3D unsteady two-phase flow in the filling cavity in oxygen of a cryogenic rocket-engine

M.-C. Gauffre[*]

Université de Toulouse; INPT, UPS; IMFT; Allée du Professeur Camille Soula, F-31400 Toulouse, France
CNRS; Institut de Mécanique des Fluides de Toulouse; F-31400 Toulouse, France
Centre National d'Études Spatiales; DLA; 52, rue Jacques Hillairet, 75612 Paris Cedex, France

H. Neau [†] O. Simonin [‡] R. Ansart [§]

Université de Toulouse; INPT, UPS; IMFT; Allée du Professeur Camille Soula, F-31400 Toulouse, France
CNRS; Institut de Mécanique des Fluides de Toulouse; F-31400 Toulouse, France

N. Meyers [¶]

Snecma Vernon; Forêt de Vernon, BP 802 - 27208 Vernon Cedex, France

S. Petitot [‖]

Centre National d'Études Spatiales; DLA; 52, rue Jacques Hillairet, 75612 Paris Cedex, France

The feeding of the LOX dome of a cryogenic rocket-engine is a decisive stage of the transient engine ignition. However flight conditions are difficult to reproduce by experimental ground tests. The work reported here is part of an ongoing research effort to develop a robust method for prediction and understanding the LOX dome feeding. In the framework of this project, experiments with substition fluids (air and water) are conducted, without mass and energy transfer. This work presented here intends to reproduce these experiments through incompressible two-phase flow CFD simulations, in an industrial geometry equivalent to the experimental mock-up, made up of a feeding piper, a dome and 122 injectors. More precisely, the aim is to compare the numerical results obtained with NEPTUNE_CFD code with the experimental results, through the dome pressure and the mass flow rate of water at the outlet. An important work was made to obtain the same inlet conditions in NEPTUNE_CFD code as the experimenters, in order to compare the numerical results with the experimental results for the best. The influence of the interfacial momentum transfer modeling and turbulence modeling are also studied here. The turbulence modeling plays no macroscopic or local role on the mass flow rate of water, on the mass of water in dome and on the dome pressure. The drag model has a major impact on our results as well globally as locally, unlike the turbulence modeling. The Simmer-like model is prefered in comparison to the Large Interface called LIM, because it is in better agreement with experimental data. Moreover, it has to be highlighted that the Simmer-like model is very sensitive to its parameter d, the inclusion diameter.

---

[*]PhD Student, Institut de Mécanique des Fluides de Toulouse; Allée du Professeur Camille Soula, F-31400 Toulouse, France.
[†]Research engineer, Institut de Mécanique des Fluides de Toulouse; Allée du Professeur Camille Soula, F-31400 Toulouse, France.
[‡]Professor, Institut de Mécanique des Fluides de Toulouse; Allée du Professeur Camille Soula, F-31400 Toulouse, France.
[§]Assistant professor, Laboratoire de Génie Chimique; Allée du Professeur Camille Soula, F-31400 Toulouse, France.
[¶]Research engineer, Snecma Vernon, BP 802 - 27208 Vernon Cedex, France.
[‖]Research engineer, Centre National d'Études Spatiales; DLA; 52, rue Jacques Hillairet, 75612 Paris Cedex, France.

Nomenclature

We Weber number
σ Surface tension, N/m
k Number of phase
ρ Density, kg/m^3
μ Dynamic viscosity, Pa.s
ν Kinematic viscosity, m^2.s
m Mass, kg
Q Mass flow rate, kg/s
α Volume fraction
θ Opening angle of the bushel valve, °
χ Fraction of wet injectors
d Inclusion diameter, m

I. Introduction

The feeding of the LOX dome of a cryogenic rocket-engine is a decisive stage. Indeed, the flow in the cavity governs the way the combustion chamber is supplied from the opening to the closure of the main valve. In particular, in the first moments of the filling of the cavity, the distribution of the flow in the injection plate region controls the ignition phase of the engine. Thus, it is necessary to know the transient flow within the injection cavity in order to provide the correct boundary conditions to simulate correctly the ignition of a cryogenic engine. As soon as the main valve is opened, the liquid oxygen enters the cavity, already swept by a helium venting at ambient temperature. In contact with the cavity walls and the helium, the liquid oxygen vaporizes strongly at first and then in a more moderate way afterwards. Therefore, the topology of the flow within the cavity evolves significantly in the first instants of its filling. Moreover, in the case of an upper-stage rocket-engine, the filling is affected by both the flashing phenomenon and the microgravity which can modify the heat transfers. Flight conditions are difficult to reproduce by experimental ground tests: CNES (Centre National d'Études Spatiales) and SAFRAN Snecma set up a research program based on both experimental and numerical studies.

It involves comparing numerical results obtained with CFD codes with the experimental work performed at LEGI (Geophysical and Industrial Flows Laboratory at Grenoble, France). Several CFD codes were foreseen: on the one hand, industrial codes like Fluent, Star-CD or CFX and on the other hand, R&D codes like NEPTUNE_CFD, CEDRE, AVBP or LEONARD. Finally two R&D codes were retained: LEONARD[1,2] code developed at Polytech Marseille (France) and NEPTUNE_CFD code developed at IMFT (Fluid Mechanics Institute at Toulouse, France). Previous works[3] showed good potential of NEPTUNE_CFD code for the simulation of the feeding of the LOX dome. In this paper the numerical results obtained with NEPTUNE_CFD code are presented. The framework is the following: substition fluids (air and water) are used and the cases studied are adiabatic, without mass and energy transfer. The aim of this research work is to simulate the filling of the cavity.

II. Experimental setup

An experimental program has been set up at LEGI in order to study the flow in the cavity, without flashing phenomenon. The matter at issue is both to understand and to identify the phenomena at stake in the transient feeding of the cavity and to build a database, so as to validate the developments in NEPTUNE_CFD models. Thus, a series of test campaigns was carried out on an experimental test bed set up at LEGI.

A. Description of the experimental setup

The LOX cavity of the rocket-engine represented in a simplified manner at LEGI by the mock-up with a toric volume which keeps the volume of the real cavity can be seen in figure 1. In addition, this experimental
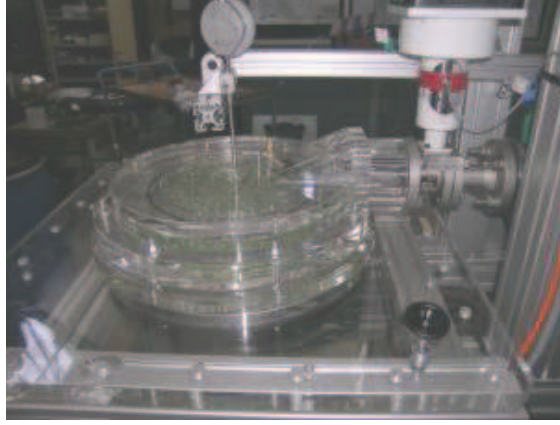
Figure 1: Experimental mock-up at LEGI.

model is made up of a cavity (also called dome), a feeding pipe upstream from the cavity, 122 injectors downstrean from the cavity and an igniter pipe in its centre.

B.   Experimental conditions

The experiment consists of a representative model of the injection cavity filled with substitution fluids respecting Weber number defined by $We = \frac{\rho_1 V_{Max}^2 D}{\sigma}$, where ρ_1 is the density of water, V_{max} is the supposed maximum inlet velocity of water when the valve is completely open, D is the diameter of the valve and σ is the surface tension. Water is the filling fluid, whereas air is the fluid initially in the cavity and also used to sweep this former. Moreover, these experiments were carried out without heat and mass transfer: dome wall are not heated and the two fluids are at the same temperature. Water flow at feeding pipe inlet level is controled by a spherical bushel valve, which ideally opens between 0° and 90° linearly during the 100 ms of the opening stage. Then during the plateau stage of 500 ms, the valve remains open at its maximum angle 90°, before closing in 500 ms until the complete closing. It has to be mentioned that during the motion of the bushel valve, the liquid entry only begins after a valve rotation of 19.6° from the closed position of the valve: this is the real beginning of the valve.

C.   Measurements carried out at LEGI

During the experiments at LEGI,[4] several measurements were carried out with a complete opening of the bushel valve. Pressure was measured in the cavity. Moreover, imaging techniques in white light were used to visualize the flow in the transparent, PMMA-made cavity. Imaging techniques by laser sheet also permitted to visualize the injectors outlet: the laser sheets detect if water comes out of the injector outlet and therefore it is possible to determine if the injectors are "wet" or not. It is to be noted that this process can not detect more than 70 "wet" injectors, for the moment.

III.   Description of CFD model

The three dimensional numerical simulations were performed with NEPTUNE_CFD v1.08.

A.   Solver and models

1.   Overall presentation of NEPTUNE_CFD

NEPTUNE_CFD is developed in the framework of the NEPTUNE project, financially supported by CEA (Commissariat à l'Énergie Atomique), EDF (Électricité de France), IRSN (Institut de Radioprotection et de Sûreté Nucléaire), and AREVA-NP. This code is a Finite Volume Eulerian multi-phase solver parallelized[5] designed for nuclear engineering.

The behavior of a fluid continuum made of several physical phases or components can be modeled using the general Eulerian multi-field balance equations[9,10,11]. Considering the adiabatic case without mass and energy transfer, the two-fluid balance equations (mass conservation and momentum conservation) are obtained from the fundamental conservation laws of physics. In our simulations, $k = 1$ is for liquid phase and $k = 2$ is for gas phase.

In NEPTUNE_CFD code[12,13], the conservation laws are written in a classical differential form that is valid at any time and location within the continuum, except across the interfaces between two physical phases. At the interfaces, jump conditions are derived from the continuous equations.

2. Balance equations

Mass balance

The multi-fluid mass balance equation for the field k writes:

$$\frac{\partial}{\partial t}(\alpha_k \rho_k) + \frac{\partial}{\partial x_i}(\alpha_k \rho_k U_{k,i}) = 0, \tag{1}$$

where α_k is the volume fraction of phase k, ρ_k is the density of phase k and $U_{k,i}$ is the ith component of the mean velocity of phase k. Total volume conservation leads to $\sum_k \alpha_k = 1$.

Momentum balance equation

The multi-fluid momentum balance equation for the field k is written in its semi-conservative form (all the contributions are conservative, except the pressure gradient one) as:

$$\frac{\partial}{\partial t}(\alpha_k \rho_k U_{k,i}) + \frac{\partial}{\partial x_j}(\alpha_k \rho_k U_{k,i} U_{k,j}) =$$

$$\frac{\partial}{\partial x_j}(\alpha_k \tau_{k,ij} + \Sigma_{k,ij}^{Re}) - \alpha_k \frac{\partial P}{\partial x_i} + \alpha_k \rho_k g_i + \sum_{p \neq k} I_{(p \to k)} + \alpha_k S_k, \tag{2}$$

where:

- P is the mean pressure, μ_k is the dynamic viscosity and g_i is the acceleration due to gravity.

- $\tau_{k,ij} = \mu_k \left(\frac{\partial U_i}{\partial x_j} + \frac{\partial U_j}{\partial x_i} - \frac{2}{3} div(U) \delta_{ij} \right)$ is the viscous stress tensor.

- $\Sigma_{k,ij}^{Re} = -\alpha_k \rho_k \left\langle U'_{k,i} U'_{k,j} \right\rangle_k$ is the turbulent stress tensor.

- S_k is the ith component of the external source term of head losses.

- $I_{(p \to k)}$ represents the ith component of the average interfacial momentum transfer rate from phase p to phase k, that accounts for the drag force. It verifies $I_{(p \to k)} + I_{(k \to p)} = 0$.

3. Closure laws in NEPTUNE_CFD

After having averaged the instantaneous local balance equations, the two-phase flow system has four main unknowns in our case: the volume fraction α_k of phase k, the mean pressure P and the mean velocity U_k of phase k.

Two terms resulting from the transition to the time-average of the instantaneous local balance equations have to be modeled in NEPTUNE_CFD in order to resolve the balance equations: the turbulent stress tensor $\Sigma_{k,ij}^{Re}$ and the interfacial momentum transfer rate $I_{(p \to k)}$.

Turbulence modeling

In our case, the k-ε turbulence model is activated for both phases. The Reynolds stresses tensor is closed for each phase, using a Boussinesq-like hypothesis:

$$\rho_k \left\langle U''_{k,i} U''_{k,j} \right\rangle_k = -\mu_k^t \left[\frac{\partial U_{k,i}}{\partial x_j} + \frac{\partial U_{k,j}}{\partial x_i} \right] + \frac{2}{3} \delta_{ij} \left[\rho_k q_k^2 + \mu_k^t \frac{\partial U_{k,m}}{\partial x_m} \right] \tag{3}$$

where μ_k^t is the turbulent viscosity and $q_k^2 = \frac{1}{2} \left\langle U_{k,i}'' U_{k,i}'' \right\rangle_k$ is the turbulent kinetic energy of phase k.

As the flow is complicated, this kind of model should be sufficient, in particular for the stratified flow.

Interfacial momentum transfer and drag closure law

In our case, only the drag force is activated for the modeling of the average interfacial momentum transfer rate $I_{(p \to k)}$.

The standard choice provided by NEPTUNE_CFD is the Simmer-like model.[6] The Simmer-like law is fitted to have a physical behaviour in the limits: it considers either dispersed gas bubbles in a continuous liquid flow or dispersed liquid droplets in a continuous gas flow with regard to the volume fraction. Thus, the Simmer-like law corresponds to the liquid droplets drag law in a continuous gas flow when the volume fraction is lower than 0.3 and to the gas bubbles drag law in a continuous liquid flow when the volume fraction of water is greater than 0.7. For intermediate volume fractions, the drag law is calculated by cubic interpolation between these two limits. The drag force F by mass unit is given by the following equations:

$$ F = F_l = -\frac{3}{4} \frac{\rho_g}{\rho_l} \frac{C_{Dl}}{d_l} |U_{rel}| U_{rel} \qquad \text{if } \alpha_l \leq 0.3, \tag{4} $$

$$ F = F_g = -\frac{3}{4} \frac{\rho_l}{\rho_g} \frac{C_{Dg}}{d_g} |U_{rel}| U_{rel} \qquad \text{if } \alpha_l \geq 0.7, \tag{5} $$

$$ F = f\left(F_l(\alpha_l = 0.3), F_g(\alpha_l = 0.7)\right) \qquad \text{if } 0.3 \leq \alpha_l \leq 0.7, \tag{6} $$

where α_l is the volume fraction of liquid, ρ_l and ρ_g are respectively the density of liquid and gas, d_g and d_l represent respectively the characteristic diameter of droplets and bubbles, U_{rel} is the relative velocity between the two phases, f defines the cubic interpolation, and C_D is the drag coefficient. This coefficient is defined by:

$$ C_D = \frac{24\nu_c}{|U_{rel}| d_p} \left(1 + 0.15 \left(\frac{|U_{rel}| d_p}{\nu_c} \right)^{0.687} \right), \tag{7} $$

where the index p corresponds to the dispersed phase and the index c to the continuous phase, and where ν is the kinematic viscosity.

Nonetheless, this model is not adapted to pure stratified flows, because the Simmer-like law may lead to a significant over-evaluation or under-estimation of the friction between the gas and the liquid. Indeed, the drag model based on the friction between a dispersed and a continuous phase is sensitive to the diameter value. So an alternative to model the friction is the Large Interface Model or LIM[7] implemented in NEPTUNE_CFD code and validated by EDF R&D from experimental measurements.[8] This method allows to locate the free surface and takes into account momentum and turbulence exchanges between phases. First the free surface is located and built from the local gradient of volume fraction, thanks to the refined-gradient method. Then in this three-cell layer built around the interface, liquid and gas characteristic tangential velocities are determined, in order to calculate interfacial velocity and momentum exchange, considering wall-function on both sides.

B.   Numerical setup

For the simulations, incompressible two-phase flow (with water and air) are considered for each phase, without mass and energy transfer. It should be remembered that NEPTUNE_CFD code solves the mass balance and the momentum balance equations for each phase. The k-ε turbulence model is activated for both phases. The dome is initially filled with air. Water is injected at pipe inlet level.

1.   Computational domain

The simulations are conducted on an unstructured three-dimensional mesh depicted in figure 2.

This mesh is the result of the merging of non coincident meshes, composed of 1,124,000 cells (mainly hexahedra). Because of the complexity of the geometry, the use of an unstructured mesh is needed. The geometry is equivalent to the experimental mock-up. This industrial geometry is composed of a feeding pipe, a cavity with 122 injectors and an igniter pipe in its centre.
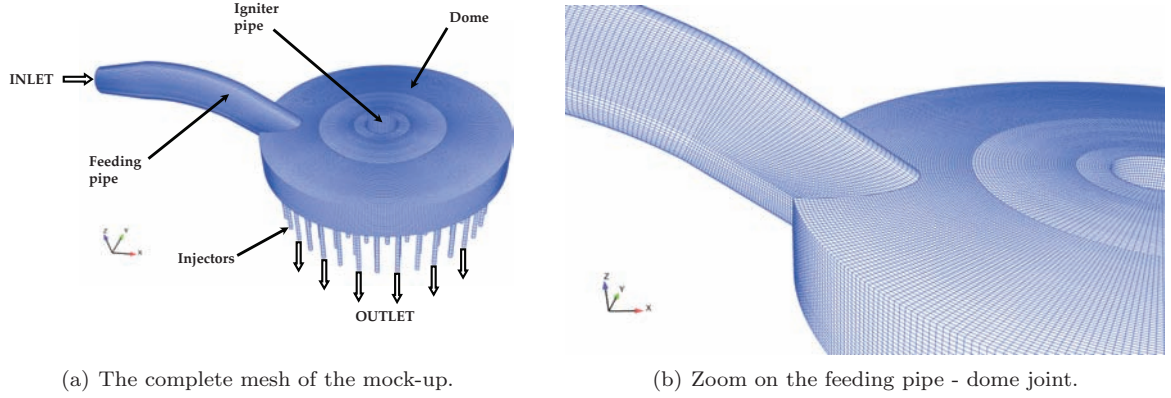
(a) The complete mesh of the mock-up.

(b) Zoom on the feeding pipe - dome joint.

Figure 2: Three-dimensional mesh for the simulations.

2. Initial conditions

The mock-up is initially filled with air (in phase $k = 2$). The density of air is $\rho_2 = 1.2$ kg/m^3 and the dynamic viscosity of water is $\mu_2 = 1.85.10^{-5}$ Pa.s.

3. Boundary conditions

Inlet boundary conditions

Water is injected at pipe inlet, with a density $\rho_1 = 1,000$ kg/m^3 and a dynamic viscosity $\mu_1 = 10^{-3}$ Pa.s. As stated before in this paper, a Weber number is imposed at the inlet: $We = \frac{\rho_1 V_{Max} D}{\sigma}$, where V_{max} is the supposed maximum inlet velocity of water when the valve is completely open, D is the diameter of the valve and σ is the surface tension. If the k-ε turbulence model is activated, this Weber number imposes the turbulent kinetic energy $q_1^2 = \frac{3}{2}(V_{Max}I)^2$ and the turbulent dissipation $\varepsilon_1 = C_\mu (q_1^2)^{3/2} l^{-1}$, where I is the turbulent rate imposed at inlet, $C_\mu = 0.09$ and $l = 0.03 D_H$ with D_H the hydraulic diameter. This injection takes into account the complete opening between 0° and 90° of the bushel valve to be in the same conditions as the experiments at LEGI. It implies that the evolution of the direction of the velocity-vectors, of the inlet opening surface area and of the mass flow rate have to be considered.

The inlet experimental data are the inlet mass flow rate of water and the opening angle θ of the bushel valve. Thus, there is still to determine the evolution of the opening surface area of this valve. As a first approximation, the 3D geometric problem of the valve opening is turned into a 2D problem in the same plane as the inlet mesh of the feeding pipe (figure 3).

The intersection of a fixed disc and a mobile disc in two different planes becomes the intersection of a fixed disc and a mobile ellipse in the same plan. This ellipse is the projection of the mobile disc onto the plane of the fixed disc and evolves during the time (in particular the position of its centre $0'$ and the dimension of its half-small axis called r). After some calculations, the area S_{Exp} of the intersection surface is:

$$
S_{Exp} = R^2 cos^{-1}\left(\frac{d}{R+r}\right) - \frac{R^2 d}{R+r} sin\left(cos^{-1}\left(\frac{d}{R+r}\right)\right)
$$
$$
+ \frac{1}{2}cos^{-1}\left(\frac{d}{R+r}\right)(r^2+R^2) - \frac{R^2-r^2}{4}sin\left(2cos^{-1}\left(\frac{d}{R+r}\right)\right) - \frac{rdR}{R+r}sin\left(cos^{-1}\left(\frac{d}{R+r}\right)\right), \quad (8)
$$

where:

- θ is the opening angle of the bushel valve,

- D is the diameter of the valve,

(a) The 3D geometric problem of the valve.   (b) The simplified 2D approach.
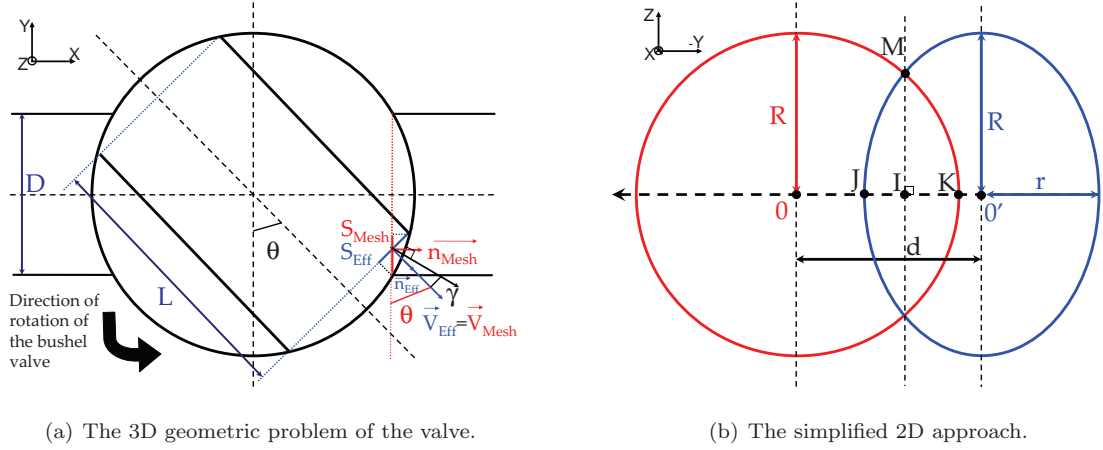
Figure 3: The 3D geometric problem of the valve turned into a 2D problem in the same plane.

- $R = \frac{D}{2}$ is the radius of the valve,

- L is the path length of the valve,

- $d = \frac{L}{2}cos\theta$ is the distance between the centre of the disc and the ellipse one,

- $r = \frac{D}{2}sin\theta$ is the half-small axis of the projected ellipse.

Actually the evolution of the opening surface area S_{Exp} is expressed in function of θ, the opening angle of the bushel valve. As the opening law of the valve is provided by the experimental data at LEGI, the time evolution of the experimental opening surface area S_{Exp} (calculated "theoretically") can be deduced.

The second issue is that the inlet mesh of the pipe is discrete. Thus, it is needed to determine which cells are well in the open inlet area of the valve, called S_{Num}. For that, the open inlet area cells are detected thanks to a second reduction: these cells are in the open area if they are a part of an ellipse area whose centre is I, whose half-small axis is $\frac{1}{2}JK$ and whose half-big axis is IM. Therefore, it amounts to say that the coordinates (Y,Z) of these open inlet area cells verify:

$$\left(\frac{Y - Y_I}{\frac{1}{2}JK}\right)^2 + \left(\frac{Z - Z_I}{IM}\right)^2 \leq 1, \tag{9}$$

which is then used directly by the code to assess the possible numerical opening surface area S_{Num}. By comparison of the values of S_{Num} and S_{Exp}, it can be deduced the opening times of the valve t_i, then the inlet mass flow rate of water corresponding $Q_{Exp}(t_i)$ (which is interpolated in the code) and finally the numerical velocity $V_{Num}(t_i)$ given by:

$$V_{Num}(t_i) = \frac{Q_{Exp}(t_i)}{S_{Num}(t_i)\rho_1 cos(\alpha_{Num})}, \tag{10}$$

where $\alpha_{Num} = \frac{\pi}{2} - \theta'$ is the inlet injection angle, with $\theta' = \theta + \gamma = \theta + arctan^{-1}\left(\frac{cos(\theta)}{1+sin(\theta)}\right)$ (θ and γ are represented in figure 3 (a)). A study (not presented here) was led and reveals that the injection angle α_{Num} of the inlet velocity has few effects on our results. Therefore, α_{Num} was calculated to be the most close to the real opening of the bushel valve.

Outlet boundary condition

At each injector outlet, are imposed a free outlet pressure and a singular head loss $\Delta P = \frac{1}{2}\zeta\rho_k U_k^2$ distributed on the four bottom cells of each injector, with $\zeta = 1$ in order to model the experimental sudden expansion at the injectors outlet.

<u>Outlet boundary condition</u>
Along the walls, standard turbulent friction functions are used for both phases.

IV.   Results

The aim of this work is to compare the numerical results obtained with NEPTUNE_CFD code with the experimental data of the LEGI, in order to study the filling rate of the cavity, the mass flow rate distribution at injection and the pressure in the cavity. In this section, a reference case is first presented with comparisons to experimental results, before focusing on the influence of the turbulence modeling and on the influence of the drag models, globally and locally.

A.   Reference case and compararisons with experimental data

1.   Validation of the valve opening modelised

This first part presents the preliminary validation of the valve opening thanks to comparisons between the inlet data implemented in NEPTUNE_CFD code at IMFT and the experimental data given by the LEGI.

The figure 4 compares the experimental opening valve angle θ and the corresponding opening surface area deduced S_{Exp} to the numerical data implemented. As written before, the inlet mesh of the feeding pipe is discrete, that is why the numerical surface area S_{Num} is crenellated. The red dashdotted lines on these graphs represent the different instants of the position of the bushel valve: the first one for the effective beginning of the valve opening ($\theta = 19.6°$ at $t = 0.123$ s), the second one when the valve is completely open ($\theta = 90°$), the third one when the valve begins to close up to $\theta = 19.6°$, which is marked by the last red line. When $\theta < 19.6°$, the valve is effectively closed and there is no inlet mass flow rate of water. Therefore, the numerical simulations really start when $\theta = 19.6°$ (at t = 0.123 s) to spare time, whereas the experiments begin before at $t = 0$ s. So in the following figures, the time origin is $t = 0.123$ s, so that the figures are more clear.
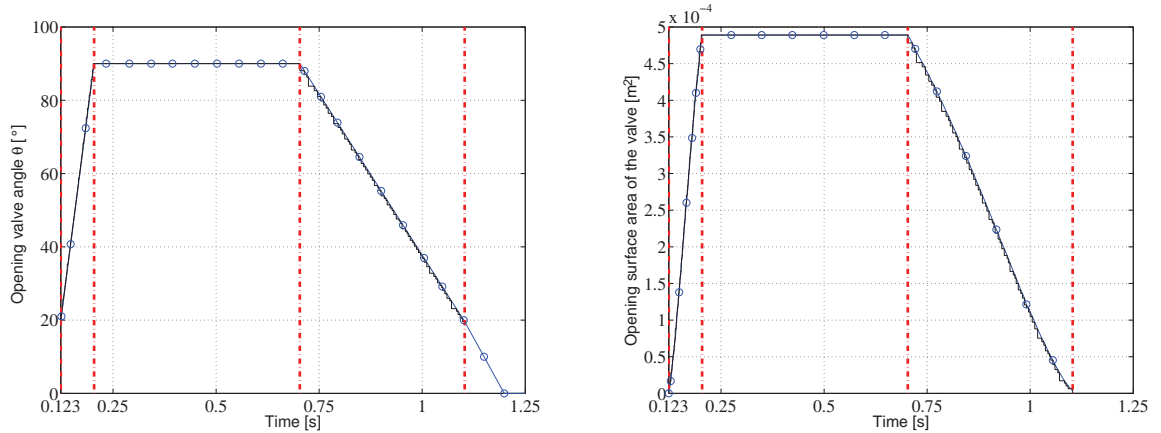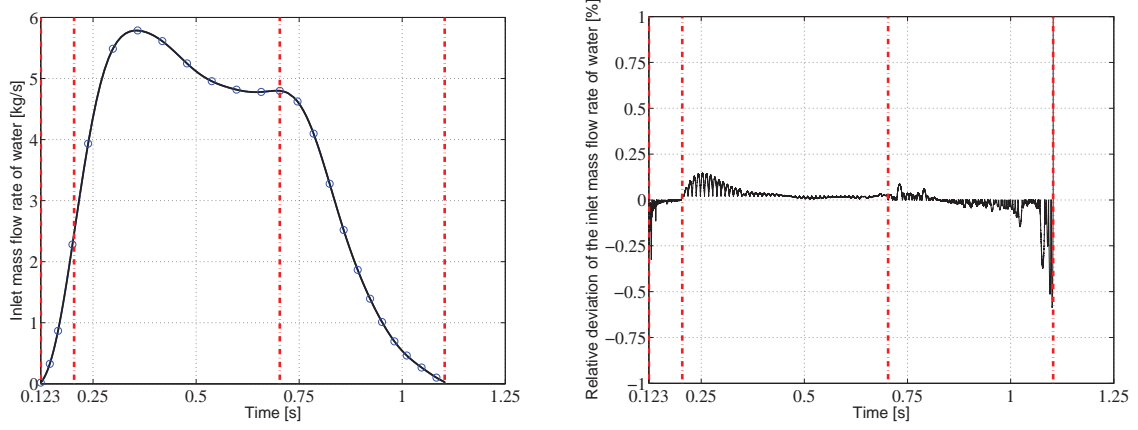

(a) Experimental and numerical opening valve angles θ.   (b) Experimental and numerical surface areas of the valve.

Figure 4: Comparisons between the experimental inlet data and the numerical input data for the opening valve angle and surface area. ──○──: Experimental inlet data, ─────: numerical inlet data, ─·──·─   : valve position.

The figure 5 shows the comparison between the experimental inlet mass flow rate and the numerical one implemented in NEPTUNE_CFD code. It can been seen in figure 5(b) the relative deviation of the inlet mass flow rate of water defined by $\frac{Q_{Exp}-Q_{Num}}{Q_{Exp}} \times 100$. Their values are included between -1% et 1%, what proves good agreement between experimental and numerical inlet data.

In figure 6 is compared the experimental inlet velocity deduced by $V_{Exp} = \frac{Q_{Exp}}{\rho_1 S_{Exp}}$ to the numerical inlet velocity V_{Num}. The inlet velocity is in good agreement with the experimental inlet velocity deduced during

(a) Evolution of the experimental and numerical inlet mass flow rate of water.

(b) Evolution of the relative deviation of the inlet mass flow rate of water.

Figure 5: Comparison between the experimental inlet data and the numerical input data for the mass flow rate of water. —o— : Experimental inlet data, ——— : numerical inlet data, —·—·— : valve position.

the opening valve and in perfect agreement when the valve is completely open. Nonetheless it can be noticed deviation from the experimental inlet velocity during the closing phase. Indeed, the inlet opening surface area being discrete, gaps of inlet velocity can be observed during this phase.Future improvements will allow S_{Num} to be even closer to S_{Exp}, like this these velocity jumps will be reduced.
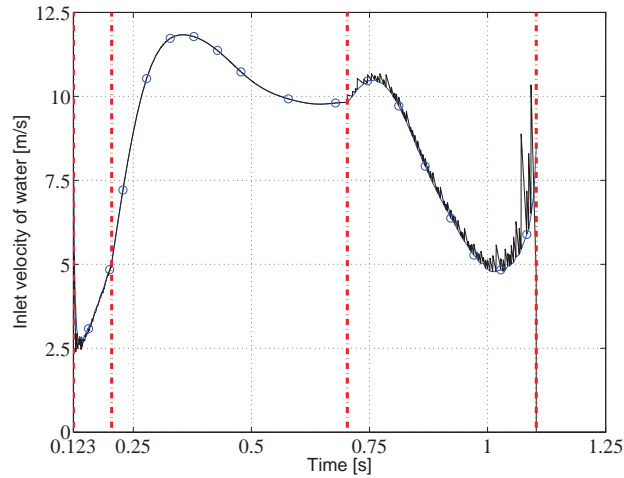
Figure 6: Comparison between the experimental inlet velocity deduced and the numerical inlet velocity. —o— : Experimental inlet velocity deduced, ——— : numerical inlet velocity, —·—·— : valve position.

2. Points of comparison

To compare the numerical results with the experimental results, it is interesting to set up common points of comparison.

The first one is the pressure measured in the dome. A probe was placed at the level of the top of the dome behind the igniter in NEPTUNE_CFD code, like the experimenters at LEGI.

A second point of comparison is the evolution of the fraction of wet injectors number named χ. Experi-
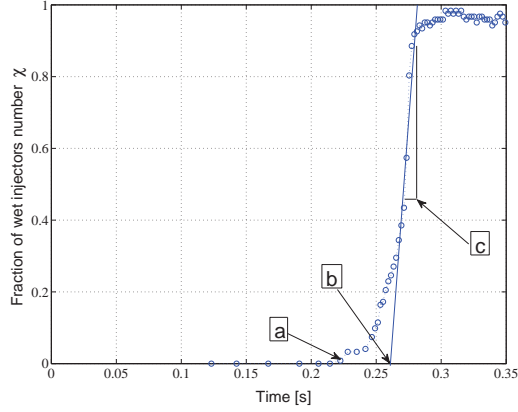
Figure 7: Representation of the three wet criteria (a, b and c) on the evolution curve of the fraction of wet injectors number.

mentally, an injector is said to be "wet" if a drop of water is detected at injector outlet by the laser sheet. Numerically this experimental criterion is not valid: it is impossible to detect a drop of water at injector outlet because the volume fraction of water is never totally null during the eulerian simulations. Therefore a numerical "wet" level is equally defined: an injector is defined as "wet" if the mass flow rate of water is bigger than a certain mass flow rate level Q_{Level}, defined as a part of the maximum outlet mass flow rate by injector. Knowing that this mock-up is made up of 122 injectors, the maximum mass flow rate by injector is $Q_{Max}/122$, where Q_{Max} is the maximum mass flow rate of water when the bushel valve is completely open. Thanks to the time evolution of the fraction of wet injectors number χ, it is possible to determine three criteria for χ :

- the date of the first wet injector, named a,

- the date of the beginning of the slope, named b,

- the slope of injection, named c.

As an example, the evolution of the fraction of wet injector number is represented in figure 7, with the three wet criteria a, b and c.

Besides, the LEGI has determined a wet law which permits to have an approximation of the evolution of the fraction of wet injectors number.[4] This law is given by :

$$\chi(t) \quad = \quad 0 \quad \text{si } t \leq \tau_{inj}^0, \tag{11}$$

$$\chi(t) \quad = \quad \frac{t - \tau_{inj}^0}{\tau_{inj}} \quad \text{si } \tau_{inj}^0 \leq t \leq \tau_{inj}^0 + \tau_{inj}, \tag{12}$$

$$\chi(t) \quad = \quad 1 \quad \text{si } t \geq \tau_{inj}^0 + \tau_{inj}, \tag{13}$$

where: $\tau_{inj}^0 = 3.4 \, \tau_0 (\frac{T_0}{\tau_0})^{0.75}$, $\tau_{inj} + \tau_{inj}^0 = 3.87 \, \tau_0 (\frac{T_0}{\tau_0})^{0.68}$, $T_0 = \frac{L_0}{V_{Max}}$ with L_0 the length between the feeding pipe and the first wet injector, and V_{Max} the supposed maximum inlet velocity of water when the valve is completely open. It has to be noted that in the theorical wet law, the criterion a is the same as the criterion b. That is why, the comparisons to the numerical results will be led only on the criteria b and c.

3. Results of the reference case

The reference case presented here was performed for a Weber number $We = 4.72.10^4$, that is to say $V_{Max} = 11.5$ m/s and $Q_{Max} = 5.65$ kg/s. The k-ε turbulence model is activated. The maximum inlet velocity V_{Max} imposes the turbulent kinetic energy and the turbulent dissipation with a turbulent rate chosen at inlet I = 5%. The drag law chosen is the Simmer-like model with the inclusion diameter $d = 10^{-3}$ m.

In figure 8 are represented the inlet and outlet mass flow rates and the mass of water in dome. Until $t = 0.823$ s, the outlet mass flow rate of water is lower than the inlet one: the mass of water increases in dome and approximately occupies 90% of the dome volume to the maximum. This is the dome filling phase. Then from $t = 0.823$ s until $t = 1$ s, the outlet mass flow rate is equal to the inlet one, so the mass of water in the dome is constant. Finally, from $t = 1$ s, the outlet mass flow rate becomes higher than the inlet one: the mass of water slowly decreases in the dome. This is the emptying dome phase.
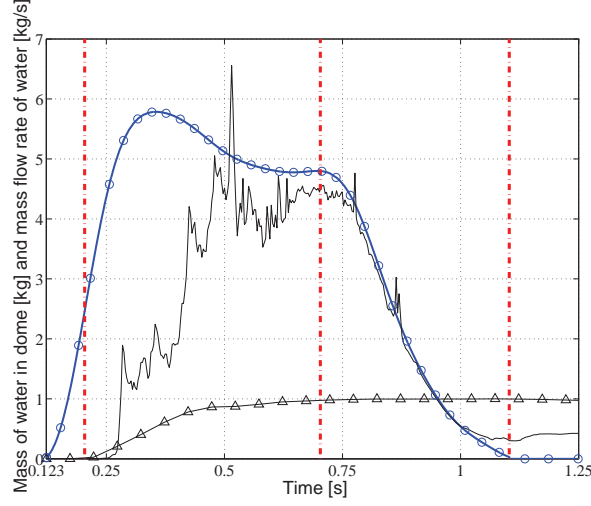
Figure 8: Numerical mass of water and mass flow rates of water. ──o── : Inlet mass flow rate, ──── : outlet mass flow rate, ──△── : mass of water in dome, ─·─·─ : valve position.

The experimental and the numerical dome pressures are depicted in figure 9. First it can be observed that the both pressures increase and decrease at the same time. Nonetheless, the numerical plateau value is different from the experimental one: on the one hand, the numerical pressure is higher than the experimantal one and on the other hand, the numerical pressure fluctuates much more. An hypothesis would be that the numerical surface area of water at injectors outlet would differ from the experimental one. A work is in perspective to study the injectors outlet and to try to understand this difference. Moreover simulations will be carried out with a compressible gas.
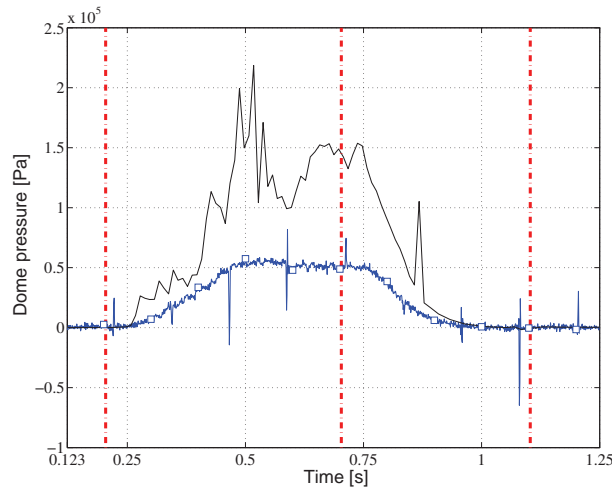

Figure 9: Comparison of the dome pressure. ──□── : Experimental pressure, ──── : numerical pressure, ─·─·─ : valve position.

After having studied globally the flow, it would be interesting to locally focus on the evolution of wet injectors to compare the numerical thresholds with the theoretical wet law. The figure 10 shows the fraction of wet injectors number χ for different level mass flow rate of water (from 0.0001% to 100%) and the theorical experimental wet law. Excepted for the threshold at 100%, there is rather good agreement between the experimental wet law and the numerical threshold chosen. Besides, the visualization of all thresholds shows that some injectors have a mass flow rate of water very big: at $t = 0.475$ s, 20% of injectors have a mass flow rate of water at 100%, whereas the 80% of one remaining have a mass flow rate at 10% or less. There is also an imbalance of the mass flow rate of water at injectors outlet.
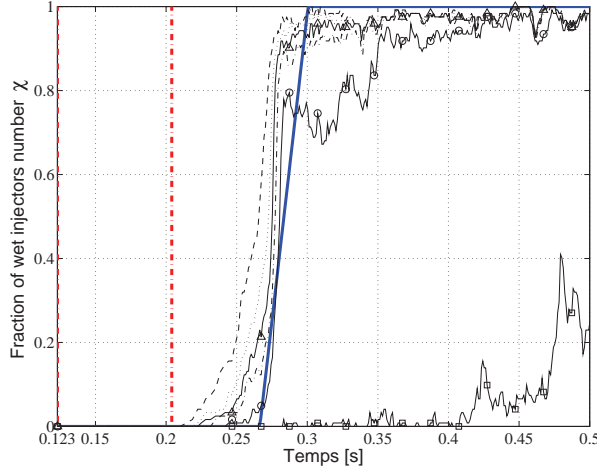

Figure 10: Comparison of the fraction of wet injectors number χ. ——— : Experimental wet law, ---- : Threshold 0.0001%, ⋯⋯⋯ : Threshold 0.01%, —△— : Threshold 0.1%, -⋅-⋅- : Threshold 1%, —∘— : Threshold 10%, —⊟— : Threshold 100%, -⋅-⋅- : valve position.

In order to have more information on the wet injectors, it can be refered to the table 1 which lists the experimental and the numerical values for criteria b and c according to the threshold chosen, and to the associated figure 11. Except the threshold at 1%, the numerical results are in very good agreement for the criterion b, which represents the beginning of the slope at the first order. Nonetheless, the relative deviation for the criteria c, which represents the slope of injection, is very great. It has to be mentioned that the experimental law is a first-order model and that the numerical slope remains subjective. Thus this criterion is not necessarily very appropriate for the comparison. It is more interesting to base oneself on the shape of the curves. For the following comparisons, all the thresholds will be considered.

B.   Influence of the turbulence modeling

A step of this work focuses on the influence of the turbulence modeling. More precisely the impact of the k-ε turbulence model is globally and locally analysed, throught three cases:

- one without turbulence modeling,

- another with k-ε turbulence model with a turbulent rate imposed at inlet I = 5%,

- a last one with k-ε turbulence model with a bigger turbulent rate imposed at inlet I = 10%.

The case presented here is performed for a Weber number $We = 4.72.10^4$, that is to say $V_{Max} = 11.5$ m/s and $Q_{Max} = 5.65$ kg/s. The drag law chosen is the Simmer-like model with the inclusion diameter $d = 10^{-3}$ m.

The turbulence modeling and the turbulent rate I have no decisive impact globally on the evolution of the outlet mass flow rate of water (in figure 12(a)). Nonetheless, observing more precisely the mass of water in dome (presented in figure 12(b)) shows a difference of behavior when the valve begins to close. Emptying the dome is a little faster without turbulence modeling.

Table 1: Influence of the threshold chosen on the criteria b and c.

| Threshold	Criteria	Numerical results	Experimental data	Relative deviation [%]
0.0001%	b [s]	0.253	0.266	4.9
	c [χ/s]	40.8	28.6	-42.7
0.01%	b [s]	0.268	0.266	-0.8
	c [χ/s]	108.5	28.6	-279
0.1%	b [s]	0.271	0.266	-1.9
	c [χ/s]	127.7	28.6	-347
1%	b [s]	0.150	0.266	43.6
	c [χ/s]	126.8	28.6	-343
10%	b [s]	0.273	0.266	-2.6
	c [χ/s]	71.7	28.6	-151
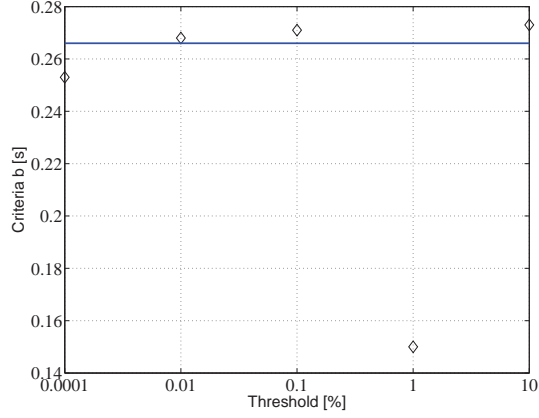
(a) Criterion b.
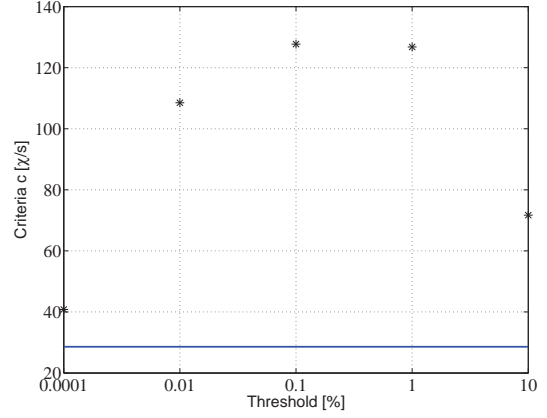
(b) Criterion c.

Figure 11: Influence of the threshold on the criteria b and c of the fraction of wet injectors number χ. ——— : Experimental values, $\diamond$: numerical criterion b, $*$: numerical criterion c.
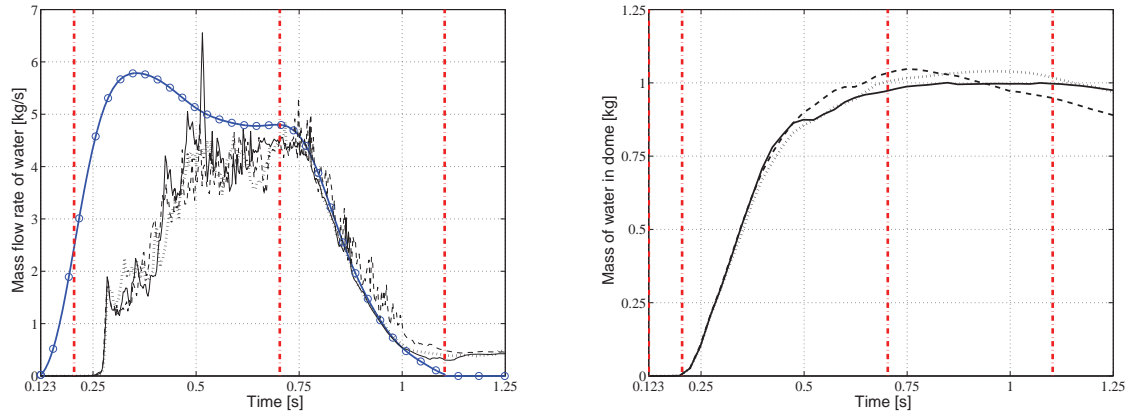
(a) Evolution of the mass flow rate of water. ——⊙—— : Inlet mass flow rate, ━ ━ ━ , ———— or ········ : Outlet mass flow.

(b) Evolution of the mass of water in dome.

Figure 12: Influence of the turbulence modeling on the evolutions of the mass flow rate of water and the mass of water in dome. ━ ━ ━ : No turbulence modeling, ———— : k-ε turbulence model with I = 5%, ········ : k-ε turbulence model with I = 10%, ━·━·━ : valve position.

There is also little influence of the turbulence modeling and of the inlet turbulent rate I on the evolution of the dome pressure, depicted in figure 13.
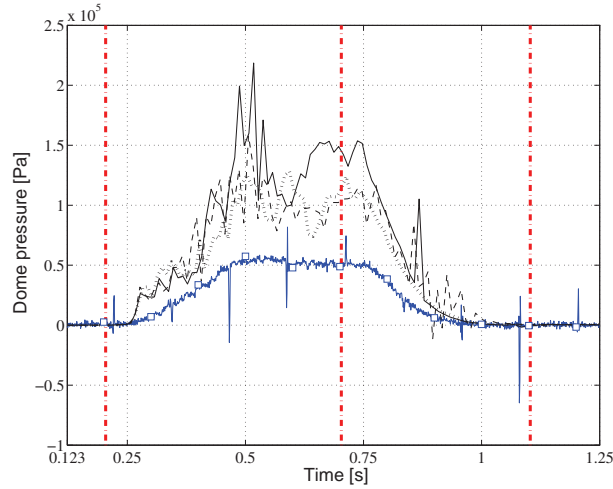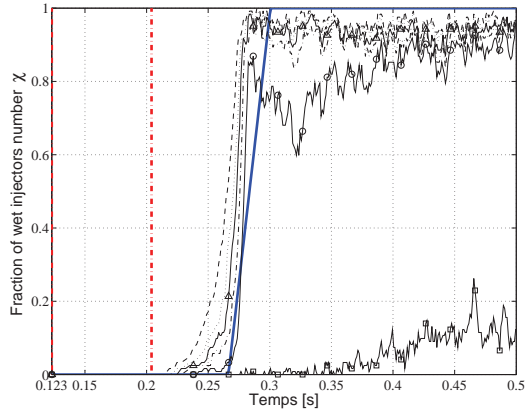

Figure 13: Influence of the turbulence modeling on the evolution of the dome pressure. —▫— : Experimental pressure, ━ ━ ━ : No turbulence modeling, ———— : k-ε turbulence model with I = 5%, ········ : k-ε turbulence model with I = 10%, ━·━·━ : valve position.
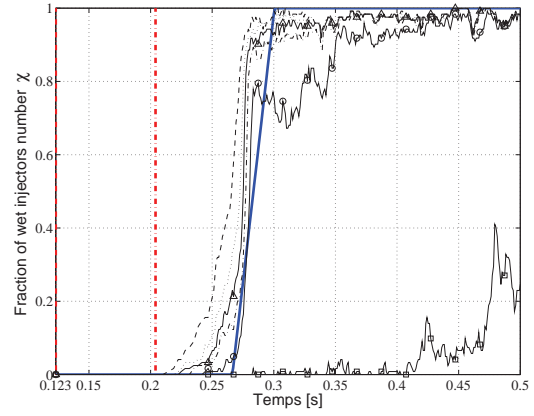
Moreover, the turbulence modeling or the turbulent rate I have also few impact on the evolution of the fraction of wet injectors number χ depicted in figure 14 and on the criteria b and c listed in table 2.

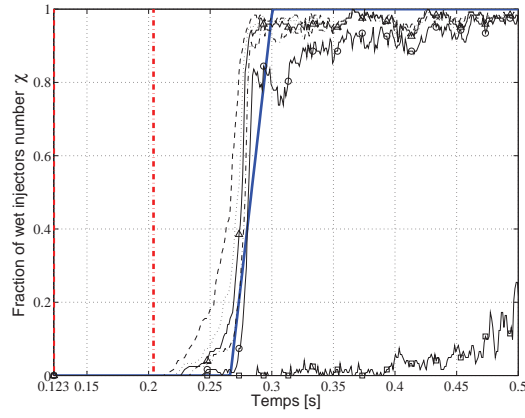In conclusion, activating the turbulence modeling or modifying the turbulent rate I play no macroscopic or local role.

(a) No turbulence modeling.

(b) k-ε turbulence model with I = 5%.

(c) k-ε turbulence model with I = 10%.

Figure 14: Influence of the turbulence modeling on the evolution of the fraction of wet injectors number χ. ——— : Experimental wet law, ---- : Threshold 0.0001%, ········ : Threshold 0.01%, —△— : Threshold 0.1%, -·--· : Threshold 1%, —◦— : Threshold 10%, —⊟— : Threshold 100%, -·--· : valve position.

Table 2: Influence of the turbulence modeling on the criteria b and c, according to the threshold chosen.

Threshold	Criteria	No turbulence modeling	k-ε turbulence model with I = 5%	k-ε turbulence model with I = 10%	Experimental data
0.0001%	b [s]	0.254	0.253	0.256	0.266
	c [χ/s]	42.5	40.8	46.3	28.6
0.01%	b [s]	0.262	0.268	0.264	0.266
	c [χ/s]	62.5	108.5	60.1	28.6
0.1%	b [s]	0.266	0.271	0.271	0.266
	c [χ/s]	80.8	127.7	104.2	28.6
1%	b [s]	0.148	0.150	0.151	0.266
	c [χ/s]	10.7	126.8	115.3	28.6
10%	b [s]	0.273	0.273	0.276	0.266
	c [χ/s]	85.8	71.7	93.4	28.6

C. Influence of the interfacial momentum transfer modeling

In this part the influence of the interfacial momentum transfer modeling is studied. First two models are tested: the Simmer-like law and the Large Interface Model called LIM. Then the influence of the particle diameter d, parameter of the Simmer-like law, is more precisely studied, the diameter at $d = 10^{-3}$ m.

The case presented here is performed for a Weber number $We = 4.72.10^4$, that is to say $V_{Max} = 11.5$ m/s and $Q_{Max} = 5.65$ kg/s. The k-ε turbulence model is activated with the inlet turbulent rate I = 5%.

1. Influence of the drag law

In this section, the influence of two drag laws are studied: the Simmer-like law (with an inclusion diameter $d = 10^{-3}$ m) and the Large Interface Model called LIM.

The evolutions of the outlet mass flow rates of water and the mass of water in dome (in figure 15) have the same behavior until 0.400 s. Then their evolutions differ: more fluctuations of the outlet mass flow rate can be observed with LIM. Moreover, the outlet mass flow of water is bigger with LIM, that is why the mass of water in dome is smaller with LIM. Until t = 0.823 s, the dome is filling before reaching a maximum filling to 80% for LIM and 90% for the Simmer-like model. After t = 0.823 s, the difference of behavior is increased between the two drag models: the dome drains off water much faster with LIM. This different behavior can be explained by a mechanical friction between liquid and gas phases lower with LIM. Indeed the exchange surface area is lower with LIM. Thus, the friction is lower and that is why the outlet mass flow rate is higher with this model.
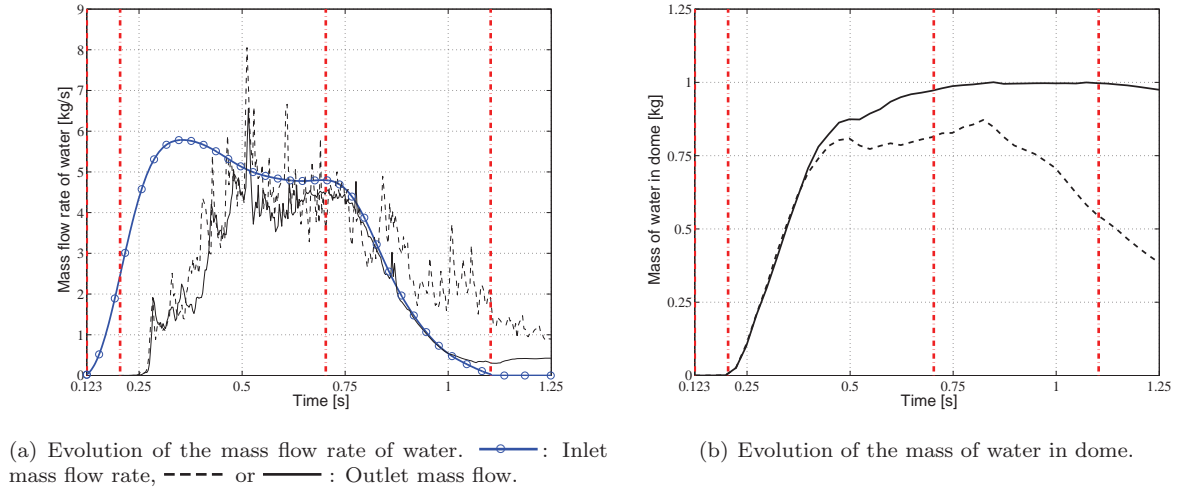

(a) Evolution of the mass flow rate of water. ──○── : Inlet mass flow rate, ---- or ──── : Outlet mass flow.

(b) Evolution of the mass of water in dome.

Figure 15: Influence of the drag law on the evolution of the mass flow rate of water and the mass of water in dome. ──── : Simmer-like model (d = 10^{-3} m), ---- : Large Interface Model, ─·─·─ : valve position.

A similar assessment can be made for the pressure in dome, depicted in figure 16. After a similar phase, the two pressures differ: the pressure with LIM is more fluctuating and bigger, because the dome is emptying faster with LIM.

The global effects highlighted before also find oneselves locally in the evolution of the fraction of wet injectors number χ, depicted in figure 17. All the injectors are not wet at the same time with LIM, contrary to the Simmer-like model. Even if the values of the criterion b which represents the date of the beginning of the slope are rather close, the values of the criterion c, the slope of injection, are always lower with LIM, as it is confirmed in the table 3.

To conclude, notable differences of behavior between the two drag models are noticed globally or locally. Thus the drag law model has a major impact on our results. Even if the Simmer-like model seems to be less physical than LIM, it would be prefered. Indeed LIM, based on a free surface detection, is in course of validation at EDF R&D: for the moment, LIM is more adapted to stationnary flows with structured mesh, contrary to our cases whose water / air interface moves fast in an unstructured mesh.
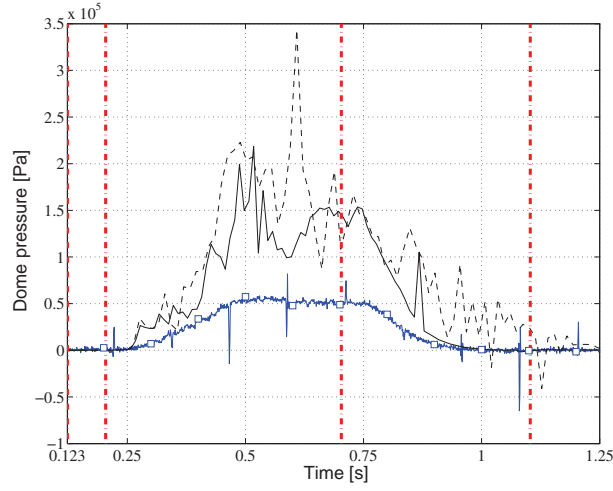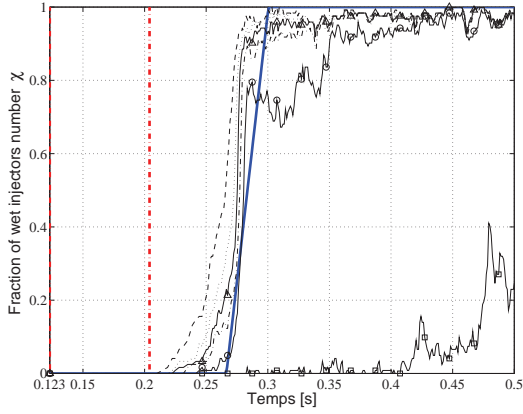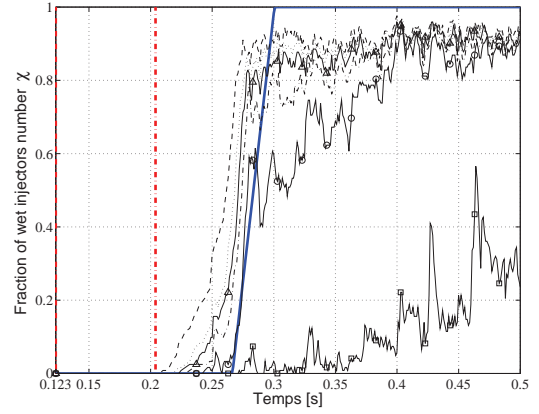
Figure 16: Influence of the drag law on the evolution of the dome pressure. □— : Experimental pressure, —— : Simmer-like model (d = 10^{-3} m), ---- : Large Interface Model, —·—·— : valve position.

(a) Simmer-like model (d = 10^{-3} m).

(b) Large Interface Model.

Figure 17: Influence of the drag law on the evolution of the fraction of wet injectors number χ. —— : Experimental wet law, ---- : Threshold 0.0001%, ········ : Threshold 0.01%, —△— : Threshold 0.1%, —·—·— : Threshold 1%, —○— : Threshold 10%, —□— : Threshold 100%, —·—·— : valve position.

Table 3: Influence of the drag law on the criteria b and c, according to the threshold chosen.

Threshold	Criteria	Simmer-like law	Large Interface Model	Experimental data
0.0001%	b [s]	0.253	0.248	0.266
	c [χ/s]	40.8	35.7	28.6
0.01%	b [s]	0.268	0.254	0.266
	c [χ/s]	108.5	38.5	28.6
0.1%	b [s]	0.271	0.261	0.266
	c [χ/s]	127.7	51.3	28.6
1%	b [s]	0.150	0.141	0.266
	c [χ/s]	126.8	51.8	28.6
10%	b [s]	0.273	0.271	0.266
	c [χ/s]	71.7	66.4	28.6

2. Influence of the inclusion diameter in the Simmer-like law

After having tested the two drag models (the Simmer-like law or the Large Inferface model), the influence of the particule diameter d, which is a parameter of this model, is studied in this part. Three diameters are tested: 10^{-5}, 10^{-4} and 10^{-3} m. It has to be noted that reducing the inclusion diameter amounts to increase the drag force (as shown in Eq. (5), (6) and (6)).

In figure 18(a) are represented the evolution of the mass flow rates of water. It has to be pointed out that the mean mass flow rate of water is the same for the three cases, let the value of the inclusion diameter. However the behavior differs as regards the mass of water in dome (figure 18(b)): there is no monotonous effect of the particule diameters on the evolution of the mass. Besides it can be noticed that the evolution of the mass of water is smoother with the lower inclusion diameter $d = 10^{-5}$ m, because the mechanical friction is bigger.
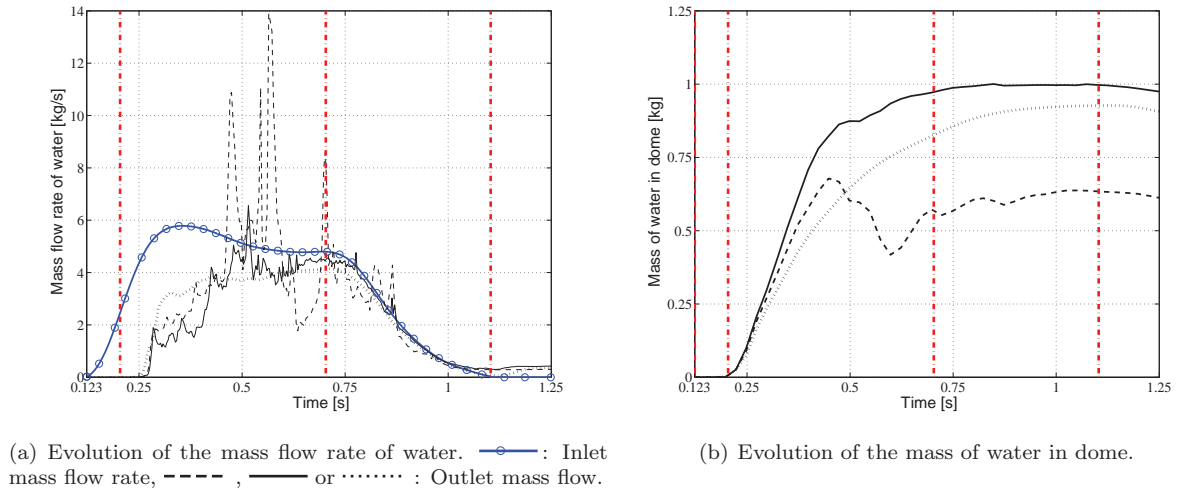

(a) Evolution of the mass flow rate of water. ─○─ : Inlet mass flow rate, ─ ─ ─ , ──── or ⋯⋯⋯ : Outlet mass flow.

(b) Evolution of the mass of water in dome.

Figure 18: Influence of the inclusion diameter in the Simmer-like law on the evolution of the mass flow rate of water and the mass of water in dome. ⋯⋯⋯ : d = 10^{-5} m, ─ ─ ─ : d = 10^{-4} m, ──── : d = 10^{-3} m, ─·─·─ : valve position.

Similarly, the evolution of the dome pressure depicted in figure 19 is not monotonous with the inclusion diameter. When d decreases, the interfacial friction increases and the pressure decreases, except for $d = 10^{-4}$ m. Actually, it would be expected that the pressure decreases with the inclusion diameter d. Indeed reducing

d shoud homogenize the water / air mixture, because the inclusions are smaller, so the exchange surface area and the friction are higher and the pressure should decrease.A case at $d = 10^{-6}$ m would confirm the trend to increase the pressure when the inclusion diameter decreases.
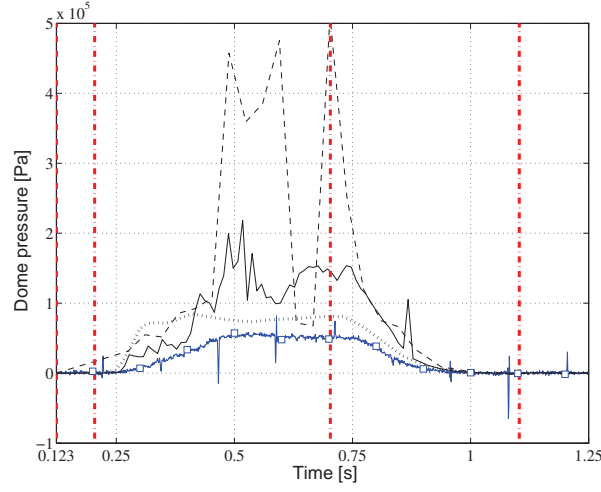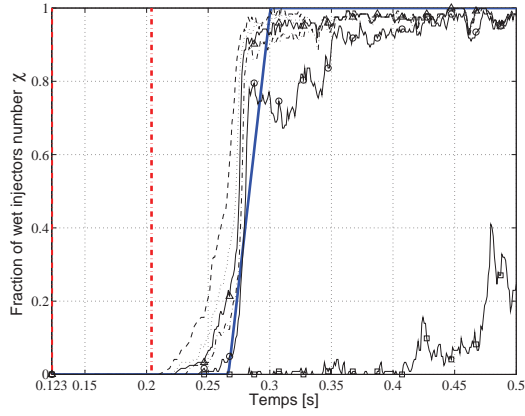

Figure 19: Influence of the inclusion diameter in the Simmer-like law on the evolution of the dome pressure. ─o─: Experimental pressure, ········ : d = 10^{-5} m, ---- : d = 10^{-4} m, ──── : d = 10^{-3} m, ─·─·─ : valve position.

The evolution of the fraction of wet injectors number χ depicted in figure 20 and the criteria b and c listed in table 4 show a weak trend of the injectors wetting to arrive earlier when the inclusion diameter deacreases. Besides, more the diameter is low, more the evolution of χ is smooth and more the maximum of χ is reached early.
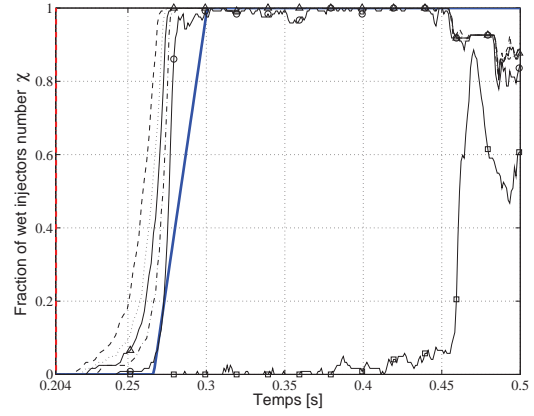
Table 4: Influence of the inclusion diameter in the Simmer-like law on the criteria b and c, according to the threshold chosen.

| Threshold	Criteria	d = 10^{-5} m	d = 10^{-4} m	d = 10^{-3} m	Experimental data
0.0001%	b [s]	0,215	0.248	0.253	0.266
	c [χ/s]	25.7	42.9	40.8	28.6
0.01%	b [s]	0,223	0.256	0.268	0.266
	c [χ/s]	31.9	54.0	108.5	28.6
0.1%	b [s]	0,235	0.260	0.271	0.266
	c [χ/s]	46.0	59.6	127.7	28.6
1%	b [s]	0.125	0.143	0.150	0.266
	c [χ/s]	70.7	81.5	126.8	28.6
10%	b [s]	0.261	0.271	0.273	0.266
	c [χ/s]	88.4	109.1	71.7	28.6

To conclude, the diameter inclusion at $d = 10^{-3}$ m seems to be in good agreement with experimental data in our case.

(a) d = 10^{-3} m.

(b) d = 10^{-4} m.
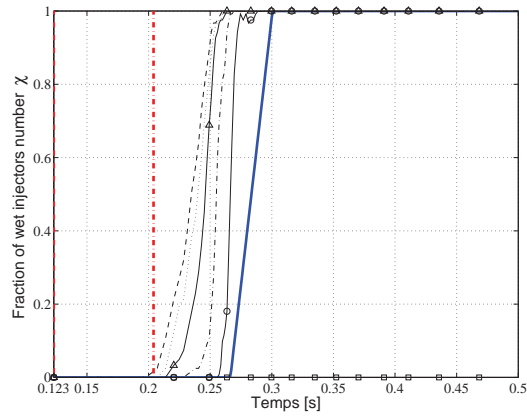
(c) d = 10^{-5} m.

Figure 20: Influence of the inclusion diameter in the Simmer-like law on the evolution of the fraction of wet injectors number χ. ——— : Experimental wet law, ‑‑‑‑ : Threshold 0.0001%, ⋯⋯⋯ : Threshold 0.01%, —△— : Threshold 0.1%, –·–·– : Threshold 1%, —o— : Threshold 10%, —☐— : Threshold 100%, –·–·– : valve position.

V. Conclusion

The feeding of the LOX dome of a cryogenic rocket-engine is a decisive stage of the transient engine ignition. However flight conditions are difficult to reproduce by experimental ground tests. The work reported here is part of an ongoing research effort to develop a robust method for prediction and understanding the LOX dome feeding. In the framework of this project, experiments with substition fluids (air and water) are conducted, without mass and energy transfer. This work presented here intends to reproduce these experiments through incompressible two-phase flow CFD simulations, in an industrial geometry equivalent to the experimental mock-up, made up of a feeding pipe, a dome with 122 injectors and an igniter.

An important work was made to obtain the same inlet conditions in NEPTUNE_CFD code as the experimenters (in particular in the modeling of the valve opening at pipe inlet level), in order to compare for the best the numerical results obtained at IMFT with the experimental results at LEGI. This work focuses also on the influence of the drag models (the Simmer-like law and the Large Interface Model called LIM) and the turbulence modeling. The turbulence modeling or the inlet turbulent rate play no macroscopic or local role on the mass flow rate of water, on the mass of water in dome and in the dome pressure. The drag model has a major impact on our results as well globally as locally, unlike the turbulence modeling. The Simmer-like model is prefered in comparison to the Large Interface called LIM, because it is in better agreement with experimental data. Moreover, it has to be highlighted that the Simmer-like model is very sensitive to its parameter d, the inclusion diameter. In our case, the diameter inclusion at $d = 10^{-3}$ m seems to be in good agreement with experimental data.

A work on the inlet boundary condition is in sight, so that the numerical inlet opening surface area S_{Num} is even closer to the experimental one S_{Exp} theoretically calculated. This will improve the numerical inlet velocity imposed in NEPTUNE_CFD code. Besides, further work will include a more specific study of the impact of the outlet boundary condition, with the addition of a tank at injector outlet, which would be more representative of the experiments at LEGI. In addition, simulations will be carried out with a compressible gas.

Acknowledgments

References

[1]R. Abgrall. How to present pressure oscillations in multi-component flow calculations: A quasi-consevative approach. Journal of Computational Physics, 1996.

[2]R. Abgrall, R. Saurel. Discrete equations for physical and numerical multiphase mixtures. Journal of Computaional Physics, 186 (2), pp 361-396, 2003.

[3]R. Ansart, R. Belt, H. Neau and O. Simonin. Dossier d'analyse physique du code NEPTUNE_CFD : Remplissage de la cavit d'injection. Technical report, IMFT, 2009.

[4]A. Cartellier, N. Hérenger and F. Mc-Cluskey. Activité LOX dôme : investigation expérimentale du remplissage de la cavité aux temps courts aux temps longs. Technical report, LEGI, 2010.

[5]H. Neau, J. Laviéville, O. Simonin. NEPTUNE_CFD High Parallel Computing Performances for Particle-Laden Reactive Flows, 7th International Conference on Multiphase Flow, ICMF, Tampa (USA), 2010.

[6]N. Méchitoua, B. Jennesson, J.-P. Schneider, M. Luck, E. Valette. Assessment of NEPTUNE_CFD code for some free Surface Flows interesting Fluvial Hydraulic, 7th International Conference on Multiphase Flow, ICMF, Tampa (USA), 2010.

[7]J. Laviéville and P. Coste. Numerical simulation of liquid-gas stratified flows using two-phase eulerian approach. FVCA5, 2009.

[8]J. Fabre, L. Masbernat and C. Suzanne. Stratified flows, part i: local structure. Multiphase science ans Technology, 3, pp. 285-301, 1987.

[9]D.A. Drew. Mathematical modeling of two-phase flow, Ann Rev. Fluid Mech, Vol. 15, pp 261-291, 1983.

[10]O. Simonin. Modélisation numérique des écoulements turbulents diphasiques à inclusions dispersée, École de printemps de Mécanique des Fluides Numérique, Aussois, 1991.

[11]O. Simonin and R. Bel F'Dhila. Eulerian prediction of a turbulent bubbly flow in a sudden pipe expansion, 6th Workshop on Two-Phase Flow Prediction, 1992.

[12]N. Méchitoua, M. Boucker, S. Mimouni, S. Pigny and G. Serre. Numerical simulation of multiphase flow with an elliptic

oriented fractional step method, Third International Symposium on Finite Volumes for Complex Applications, Porquerolles, France, 2002.

[13]N. Méchitoua, M. Boucker, J. Laviéville, J.-M. Hérard, S. Pigny and G. Serre. An unstructured finite volume solver for two-phase water / vapour flows modeling based on ellipstic oriented fractional step method, NURETH 10, Seoul, South Corea, 2003